Synchronous measurement of inertial rotation and magnetic field using a K-Rb-^{21}Ne comagnetometer

Wei Quan, Kai Wei,* Tian Zhao, Hairong Li, and Yueyang Zhai

School of Instrumentation and Optoelectronic Engineering, Science and Technology on Inertial Laboratory, Beihang University, Beijing 100191, China

(Received 3 November 2016; revised manuscript received 27 January 2019; published 15 July 2019)

We propose a method for synchronous measurement of inertial rotation and magnetic field based on the nuclear spin magnetization of the ^{21}Ne self-compensation magnetic field and enhancement of the rotation signal in a K-Rb-^{21}Ne comagnetometer. Under different working temperature conditions, we study the operation of the system as a self-compensation comagnetometer. Using the formulated Bloch equations, the magnetic field and inertial rotation are simultaneously measured by the transient and steady responses in a single probe beam configuration. The measurement of earth rotation projection on the horizontal plane from -5.59×10^{-5} to 5.59×10^{-5} rad/s based on the steady signal and measurement of the magnetic field ranging from 0.016 to 1.760 nT based on the transient signal have been presented. Furthermore, the simultaneous measurements of angular velocity varying from -4.01×10^{-5} to 5.37×10^{-5} rad/s with an accuracy of 2×10^{-5} rad/s and a magnetic field changing from 0.048 to 0.128 nT with an accuracy of 0.01 nT have also been demonstrated.

DOI: 10.1103/PhysRevA.100.012118

I. INTRODUCTION

High-precision atomic magnetometers used to measure inertial rotation and magnetic field have been applied in several fields, including tests of fundamental symmetries, inertial navigation, and biomagnetism [1–3]. In the terms of magnetic-field measurements, the optically pumped magnetometer operating in the spin-exchange relaxation-free (SERF) regime holds the magnetic-field sensitivity record of 0.16 $\mathrm{fT/Hz^{1/2}}$ as a gradiometer [4], surpassing the low-T_c superconducting quantum interference device with the sensitivity of about 1 $\mathrm{fT/Hz^{1/2}}$. Furthermore, atomic magnetometers have been developed to measure a three-dimensional magnetic field [5] and be microfabricated as chip-scale sensors [6]. As for rotation measurements, although mechanical gyroscopes and fiber-optic gyroscopes are dominant, especially for inertial navigation, the atomic spin gyroscopes developed from atomic magnetometers with sensitivity of about 5×10^{-7} $\mathrm{rad\,s^{-1}\,Hz^{-1/2}}$ have opened additional possibilities for high-precision rotation sensing [7] and demonstrated dual-axis components' measurement [8].

Although SERF atomic magnetometers and comagnetometers can achieve ultrahigh sensitivity in magnetic field and rotation measurement, the intrinsic nature that the magnetic field and rotation cause indistinguishable atom spin precession induces unexpected systematic errors in separate measurements. Especially, under the condition that the compensation point of the SERF comagnetometer is drifted, ambient magnetic-field variation induces severe systematic errors in the signal of the comagnetometer, resulting in accumulative errors in rotation measurements and local Lorentz invariance testing [7,9]. This problem can be solved by repeating the zeroing routine [9] in which the measurement is paused periodically for implementation of a magnetic-field zeroing procedure. The periodic pause in this method induces an unwanted dead zone of the measurement. Another method is to simultaneously measure the magnetic field and rotation before and extract them from the signal, respectively. A method based on separate probes of potassium (K) and rubidium (Rb) in the K-Rb magnetometer was proposed and simulated [10]. However, the difference between two probe lights is trivial due to fast spin-exchange collisions of K and Rb and is difficult to realize in practical applications.

In this paper, we propose a method for simultaneous measurement of magnetic field and rotation based on a K-Rb-^{21}neon (Ne) comagnetometer in which the nuclear magnetization of ^{21}Ne cancels slow fluctuation of ambient magnetic fields [11]. The response of the comagnetometer, both transient and steady state, is studied in detail using Bloch equations; and it fits well with experimental results. It is demonstrated that the magnetic field and rotation can be simultaneously measured by extracting information from the transient and steady responses of the comagnetometer. Our method can be used as a real-time measuring and zeroing method to avoid information lost during the experiment. It could also be used as part of close-loop magnetic-field control in a precision rotation measurement.

II. BASIC PRINCIPLE

The K-Rb-^{21}Ne comagnetometer consists of a spherical vapor cell containing a mixed droplet of alkali metal (K-Rb) and ^{21}Ne gas as well as N_2 gas. The cell is heated by an electric heater to achieve high vapor densities of alkali-metal atoms. K electron spins are directly pumped by a circularly polarized

*weikai@buaa.edu.cn

K D_1 light and used to polarize Rb atoms by spin-exchange collisions. Because the density of K atoms in this mixed alkali metal vapor is much smaller than that of a pure K vapor with the same temperature, the absorption of the K D_1 pump beam along the direction of propagation is much slighter, resulting in a much homogeneous polarization [12]. The polarization of ^{21}Ne nuclear spins is primarily generated by spin-exchange collisions with Rb atoms because the density of Rb atoms is two orders of magnitude larger than that of K [8]. The transverse component of Rb polarization, induced by the input magnetic field and inertial rotation, is measured by a linearly polarized probe light based on optical rotation.

In a K-Rb-^{21}Ne comagnetometer, the primary interactions between K and Rb atoms are spin-exchange interaction and spin-destruction interaction. At the typical operation temperature about 473 K, the densities of K and Rb atoms in the hybrid cell are about 8×10^{12} and 8×10^{14} cm^{-3}, respectively, giving a density ratio $D_r = n_K/n_R b \approx 1/100$. Due to the sufficiently large spin-exchange cross section between K-Rb, $\sigma_{\rm se}^{\rm K\text{-}Rb} = 2 \times 10^{-14}$ cm^2, the spin-exchange rate from K to Rb $R_{\rm se}^{\rm K\text{-}Rb}$ (the other way around for $R_{\rm se}^{\rm Rb\text{-}K}$) is about 1×10^4 1/s (1×10^6 1/s), which is larger than the typical 800-1/s relaxation rate of alkali-metal atoms in the K-Rb-^{21}Ne SERF comagnetometer. Hence, the Rb and K atoms are in spin-temperature equilibrium with the same spin polarization [12] and can be regarded as one spin species. The polarization of Rb atoms by spin-exchange interaction with K atoms can be represented by an effective pump light directly polarizing Rb atoms with a pump rate R_p. Besides, the K-Rb spin-destruction interaction on the Rb atom, which is several orders of magnitude smaller than that of Rb-Rb, could be considered in the spin-destruction rate of Rb atoms $R_{\rm sd}^e$. Therefore, the interactions between K-Rb could be represented by two parameters R_p and $R_{\rm sd}^e$.

As for the interactions between alkali-metal atoms and ^{21}Ne atoms, the main interactions are the spin-exchange interaction and the spin-destruction interaction. Among these interactions, the imaginary part of the spin-exchange interaction is the dominant interaction, which is several orders of magnitude larger than the others [11]. Typically, the imaginary part of the spin-exchange interaction of electron-electron, which induces the frequency shift, is smaller than the real part that causes the spin transition. However, due to the weak spin-exchange interaction between alkali-metal and noble atoms, the imaginary part is 10^5 larger than the real part. The imaginary part of spin-exchange interaction for electron-nuclear spin-exchange interaction could be described by effective magnetic fields experienced by ^{21}Ne atoms and alkali-metal atoms, respectively, due to the magnetization of the other, which are denoted as $\mathbf{B^e}$ and $\mathbf{B^n}$, respectively. Especially, in a spherical cell, this magnetic field is $\mathbf{B} = 8\pi k_0/3\, M\mathbf{P}$, where $M = \mu n$ is the magnetization for full polarization, μ is the magnetic moment, n is the density, $\mathbf{P}$ is the polarization, and k_0 is the Fermi contact shift enhancement factor [13]. As for the real part of the spin-exchange interaction, it is used to polarize the ^{21}Ne atoms over a period of several hours. Although the impact of the real part on the dynamics of the K-Rb-^{21}Ne comagnetometer is negligible, it determines the equilibrium nuclear polarization of ^{21}Ne atoms and is described by a spin-exchange rate. Besides, the spin-destruction interaction

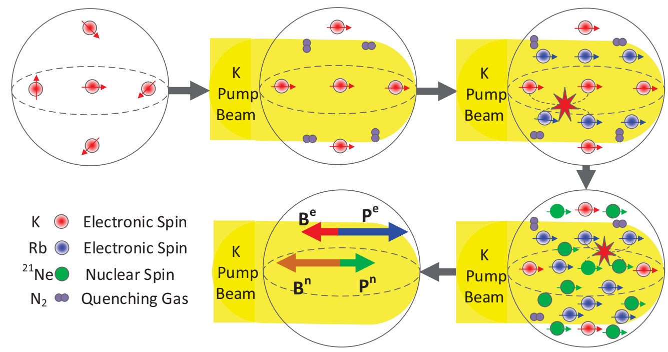

FIG. 1. Schematic of the polarization process and the simplified interaction model.

between alkali-metal and ^{21}Ne atoms is also described by a spin-destruction rate.

For the K-^{21}Ne pair and the Rb-^{21}Ne pair, the k_0's are 30.8 ± 2.7 and 35.7 ± 3.7, respectively [14]. Besides, the density ratio of K to Rb atoms is typically on the order of 10^{-2}, and the spin polarization of K equals that of Rb. Thus, the effective magnetic field experienced by ^{21}Ne atoms due to the magnetization of K $\mathbf{B_K^e}$, is two orders of magnitude smaller than that due to the magnetization of Rb $\mathbf{B_{Rb}^e}$. Therefore, the interactions between ^{21}Ne atoms and alkali-metal atoms are dominated by a Rb-^{21}Ne pair, and the interactions between K-^{21}Ne can be safely ignored. In conclusion, the K-Rb-^{21}Ne comagnetometer could be simplified to the Rb-^{21}Ne comagnetometer with the interactions associated with K atoms represented by the effective pumping and spin-relaxation rates.

The schematic of the polarization process of alkali-metal atoms and noble gas is depicted in Fig. 1 and divided into five steps. The first step shows that the K electron spins are in the random state in the initial state. The second step depicts that the disorderly K electron spins are polarized by the circularly polarized pump light, where N_2 is used as a quenching gas to suppress the radiation trapping. The third step indicates that the Rb electron spins are polarized via spin-exchange collisions with K atoms, and the alkali-metal spin ensembles reach the spin-polarization equilibrium rapidly. As shown in the fourth step, the ^{21}Ne nuclear spins are polarized by spin-exchange collisions with Rb atoms mainly because the density of Rb is two orders of magnitude larger than that of K. After several hours, the polarizations of the mixed spin ensembles approach steady state. Because the main interaction of Rb-^{21}Ne is described by the effective magnetic fields and the response of the Rb-^{21}Ne spin ensembles to input the magnetic field and rotation signals is related to their spin polarizations, the Rb-^{21}Ne spin ensembles can be represented by two vectors $\mathbf{P^e}$ and $\mathbf{P^n}$, and the effective magnetic fields can be represented by $\mathbf{B^e}$ and $\mathbf{B^n}$ for simplicity.

The dynamics of the comagnetometer could be appropriately described by the Bloch equations coupling Rb electron and ^{21}Ne nuclear polarizations $\mathbf{P^e}$ and $\mathbf{P^n}$ with spin-exchange interaction and spin-destruction interaction [7,15], whereas the interactions between K and Rb spin ensembles are represented by an equivalent pumping rate and spin-destruction rate,

$$\frac{\partial \mathbf{P}^e}{\partial t} = \frac{\gamma_e}{Q}(\mathbf{B} + \lambda \mathbf{M}^n \mathbf{P}^n + \mathbf{L}) \times \mathbf{P}^e + \mathbf{\Omega} \times \mathbf{P}^e + \frac{R_m \mathbf{S}_m + R_p \mathbf{S}_p + R_{se}^{ne} \mathbf{P}^n}{Q} - \frac{\mathbf{P}^e}{Q\{T_1, T_2, T_2\}},$$
$$\frac{\partial \mathbf{P^n}}{\partial t} = \gamma_n(\mathbf{B} + \lambda \mathbf{M}^e \mathbf{P}^e) \times \mathbf{P^n} - \mathbf{\Omega} \times \mathbf{P^n} + R_{se}^{en} \mathbf{P}^e - R_{tot}^n \mathbf{P^n}. \tag{1}$$

Here γ_e and γ_n are the gyromagnetic ratios of an electron and a ^{21}Ne nucleon, and Q is the slowing-down factor. $\mathbf{B}$, $\mathbf{\Omega}$, and $\mathbf{L}$ are the external magnetic field, the inertial rotation, and the light shift, respectively. R_p and R_m are the pumping rates of pump and probe lights, whereas $\mathbf{S_p}$ and $\mathbf{S_m}$ are their photon spins. R_{se}^{ne} is the spin-exchange rate from ^{21}Ne atoms to Rb atoms, and the other way around for R_{se}^{en}. For the Rb spin ensemble, the longitudinal and transverse relaxation rates are $T_1^{-1} = R_m + R_p + R_{se}^{ne} + R_{sd}^e$ and $R_{tot}^e = T_2^{-1} = T_1^{-1} + QR_{se}^{ee}$, respectively, where R_{sd}^e is the spin-destruction rate, and R_{se}^{ee} is the spin-exchange relaxation rate. $R_{tot}^n = R_{se}^{en} + R_{quad}^n + R_{sd}^n$ is the total spin-relaxation rate of ^{21}Ne, where R_{quad}^n is the quadrupole relaxation rate of ^{21}Ne.

The full Bloch equations are nonlinear and hard to be solved analytically. Approximation is needed to simplify the solution. For small transverse excitations, it is a fairly good approximation to assume that the longitudinal components P_z^e and P_z^n are nearly constant such that the Bloch equations could be linearized. Typically, the transverse relaxation rate of Rb atoms is about 2000 1/s, thus, for effective transverse input signals roughly about 5 nT, the longitudinal components are not affected. The transverse component P_x^e can be obtained by solving the linearized Bloch equations. Based on the optical rotation, the signal measured by the photodiode S_x^e is proportional to P_x^e by the factor K_d and is given by

$$S_x = K_d P_x^e = e^{\lambda_{1r} t}(P_{1r} \cos \lambda_{1i} t - P_{1i} \sin \lambda_{1i} t) + e^{\lambda_{2r} t}(P_{2r} \cos \lambda_{2i} t - P_{2i} \sin \lambda_{2i} t) + S_x^{steady}, \tag{2}$$

where $\lambda_1 = \lambda_{1r} + i\lambda_{1i}$ and $\lambda_2 = \lambda_{2r} + i\lambda_{2i}$ are two oscillations corresponding to precessions of Rb electrons and ^{21}Ne nuclei, respectively, with different decay rates and frequencies, which are entirely determined by the system itself and specifically formulated in our previous work [16]. P_{1r}, P_{1i}, P_{2r}, and P_{2i} depending on initial conditions and the input signals could be concretely formulated with different types of inputting magnetic-field variation and inertial rotation.

When a bias magnetic-field $B_c = -B^e - B^n$ produced by the coils is applied along the Z axis, the comagnetometer works in a regime called self-compensation that the nuclear magnetization of ^{21}Ne could arbitrarily cancel slowly changing B_y in steady state [7]. As shown in Fig. 2(a), without a transverse input signal, the Rb electron and ^{21}Ne nuclear spin-polarizations $\mathbf{P^e}$ and $\mathbf{P^n}$ are polarized along the Z axis initially. A bias magnetic-field $B_c = -B^e - B^n$ is applied along the Z axis to operate the comagnetometer at the self-compensation point. When applying a magnetic-field B_y along the Y axis, $\mathbf{P^e}$ and $\mathbf{P^n}$ would begin to precess in the transient process. After a short time, the precessions would decay to steady state. $\mathbf{P^n}$ would stabilize along the direction on the Y-Z plane, thus the projection of $\mathbf{B^n}$ on Y-axis B_y^n would compensate B_y. Because the total transverse magnetic field experienced by Rb electrons is zero $B_y^n + B_y = 0$, $\mathbf{P^e}$ would return back to the Z axis, unaffected by B_y in steady state. Besides, the principle of rotation sensing in steady state is shown in Fig. 2(b). When inputting rotation Ω_y along the Y axis, $\mathbf{P^n}$ would precess and stabilize along a direction on the Y-Z plane in steady state, thus $\mathbf{B^n}$ would produce a projected magnetic-field B_y^n along the Y axis. The effective rotation signal experienced by Rb electrons along the Y axis is the sum of Ω_y and B_y^n, which is enhanced relative to the original signal Ω_y. $\mathbf{P^e}$ would stabilize along a direction on the X-Z plane in steady state, whose projection on the X-axis P_x^e can be measured based on the optical rotation to obtain the rotation Ω_y.

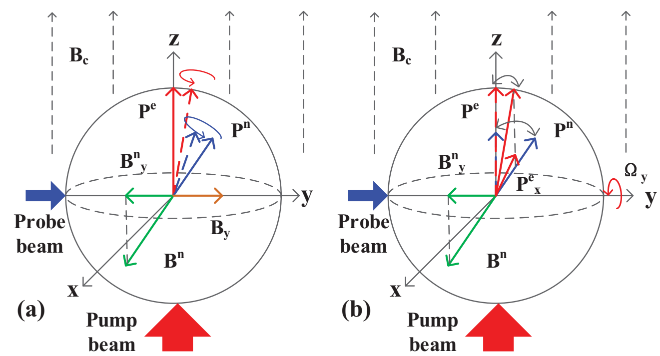

FIG. 2. Intuitive model of the basic operation.

As shown in Fig. 2, operating at the self-compensation regime, the nuclear magnetization of ^{21}Ne atoms could arbitrarily cancel slowly changing B_y in steady state, leaving the steady-state signal only proportional to rotation signal Ω_y. Although the steady-state signal is unaffected by the magnetic field, the transient signal is still related to the magnetic field and rotation both. Thus, the value of Ω_y can be obtained in a steady signal, and the value of B_y can be acquired by substituting Ω_y into the measured transient signal. When inputting a steplike magnetic field and quasistatic inertial rotation, P_{1r} and S_x^{steady} could be described as

$$P_{1r} = K_B B_y + K_\Omega \Omega_y, \tag{3}$$

$$S_x^{steady} = K_{steady}\left(\frac{\delta B_z}{B^n} B_y + \frac{\Omega_y}{\gamma_n}\right), \tag{4}$$

$$K_B = \frac{\gamma_e P_z^e}{Q} K_d \frac{\lambda_{1r} - \lambda_{2r}}{(\lambda_{2r} - \lambda_{1r})^2 + (\lambda_{2i} - \lambda_{1i})^2}, \tag{5}$$

$$K_\Omega = \frac{\gamma_e P_z^e}{\gamma_n R_{tot}^e} K_d \left[\frac{(R_{tot}^e \gamma_n/\gamma_e - \lambda_{2r})(\lambda_{2r} - \lambda_{1r})}{(\lambda_{2r} - \lambda_{1r})^2 + (\lambda_{2i} - \lambda_{1i})^2} - \frac{\lambda_{2i}(\lambda_{2i} - \lambda_{1i})}{(\lambda_{2r} - \lambda_{1r})^2 + (\lambda_{2i} - \lambda_{1i})^2}\right], \tag{6}$$

$$K_{steady} = \frac{K_d \gamma_e P_z^e R_{tot}^e}{{R_{tot}^e}^2 + {\gamma_e}^2 (L_z + \delta B_z)^2}. \tag{7}$$

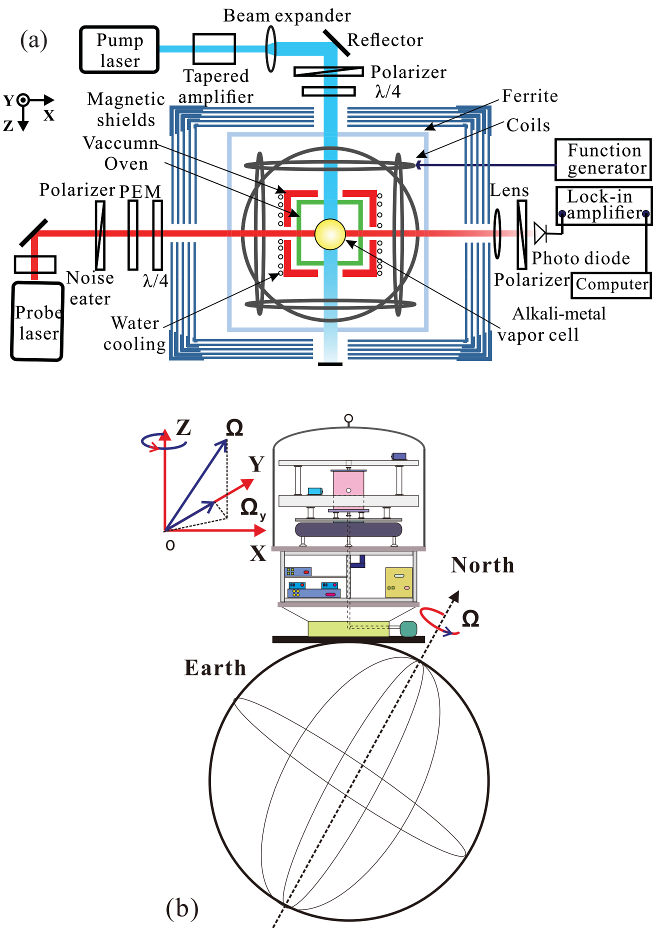

FIG. 3. (a) The schematic of the comagnetometer. (b) The diagram of measuring the earth rotation projection. The coordinates of the laboratory are north latitude 40.0° and east longitude 116.4°. The comagnetometer rotates along the Z axis, therefore, the projection of the earth rotation $\mathbf{\Omega}$ on the measurement direction of the comagnetometer Ω_y would change sinusoidally. At the beginning, the direction of the Y axis of the comagnetometer is determined by a north seeker.

Here, K_B, K_Ω, K_{steady}, λ_1, and λ_2 are system parameters determined by the system itself and could be measured by the calibration. At the self-compensation point $\delta B_z = B_z - B_c = 0$, the values of B_y and Ω_y can be obtained by fitting the complete response signal containing the transient and steady components with Eqs. (2)–(4) after determination of the system parameters.

The concrete procedures of this simultaneous measurement method are that: First, the oscillation parameters λ_1 and λ_2 are acquired by fitting the response to a step magnetic field, whereas the scale factors K_B, K_Ω, and K_{steady} are calibrated by various inputting signals. Second, these calibrated parameters are used to fit the response signal S_x to obtain magnetic-field B_y and rotation Ω_y based on Eqs. (2)–(4).

III. EXPERIMENTAL SETUP

The experimental setup is shown in Fig. 3(a). The 14-mm diameter spherical cell containing a mixture droplet of K-Rb with the density ratio of about 1:100 at 453 K, 2020 Torr of ^{21}Ne (70% isotope enriched), and 31-Torr N_2 (quenching gas) is heated by a 110-kHz AC electrical heater within a boron nitride ceramic oven, and they are installed inside a polyetheretherketone vacuum vessel. The vessel cooled by the water-cooling tube is enclosed by a ferrite barrel and a five-layer cylindrical μ metal to shield ambient magnetic field and reduce inner magnetic noise. Additionally, a three-axis coil is used to compensate the residual magnetic field [17].

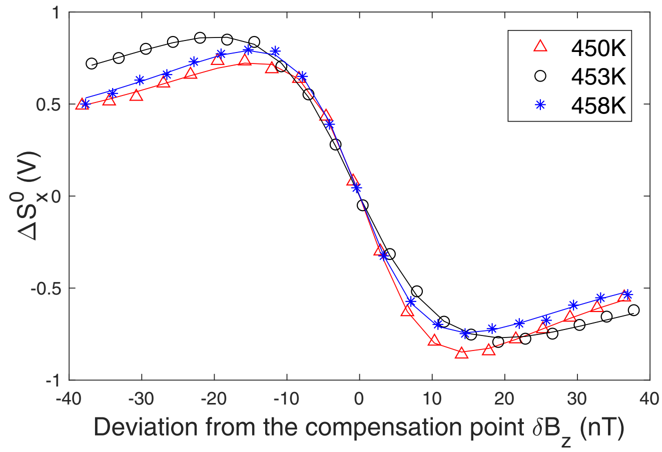

FIG. 4. The dependence of the difference between the initial and the steady state responses ΔS_x^0 on the deviation from the compensation point δB_z for different temperatures.

The pump light produced by an external cavity diode laser is tuned to D_1 resonance of K, which is amplified by a tapered amplifier to 1.2 W and expanded to cover the cell to polarize K atoms along the Z axis. The S_x component of Rb spin polarization is measured by a linearly polarized probe light propagating along the X axis from a distributed feedback laser whose wavelength is tuned to the red detuning (0.4 nm) of D_1 resonance of Rb. The probe light is modulated by a photoelastic modulator (Hinds Instrument) with the amplitude of about 0.08 rad and the frequency of about 50 kHz and demodulated by a lock-in amplifier (Stanford Research SR830).

The whole experimental setup is mounted on a rotation platform whose rotating axis (Z axis) is carefully calibrated to be perpendicular to the local horizontal plane so that the probe beam (X axis) can be directed along any direction of the horizontal plane to measure the projection of earth rotation on Y-axis Ω_y as shown in Fig. 3(b).

IV. RESULTS AND DISCUSSIONS

We first set the comagnetometer work in the self-compensation regime. To find the appropriate compensation point B_c, we record the signal response to a step magnetic-field B_y with amplitude 0.32 nT at three different temperatures. By scanning $\delta B_z = B_z - B_c$, we find the difference ΔS_x^0 between the steady signal before and the steady signal after the step magnetic field equals to zero at $\delta B_z = 0$ as shown in Fig. 4, which indicates the suppression of the magnetic field due to the projection of ^{21}Ne nuclear magnetization along the Y axis [7,11]. Experimental results agree well with fitted results from Eqs. (4) and (7). At the working temperature of

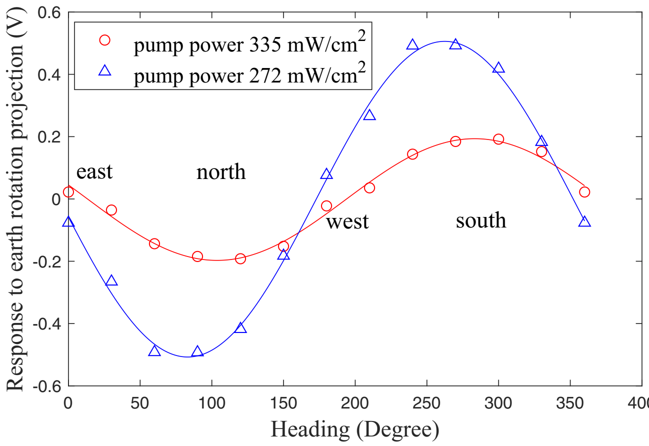

FIG. 5. The comagnetometer responses to the projection of earth rotation Ω_y with different pump power.

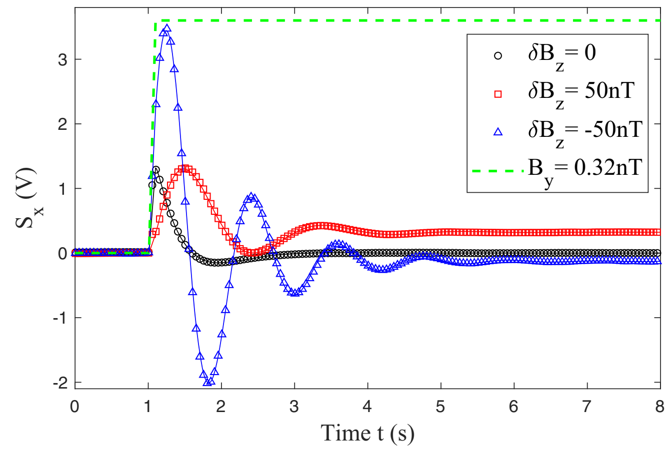

FIG. 6. The responses of the comagnetometer to a step magnetic field with various compensation fields $\delta B_z = B_z - B_c$. The measured responses with $\delta B_z = 50$, $\delta B_z = 0$, and $\delta B_z = -50$ nT are drawn in red squares, black circles, and blue triangles, respectively, and fitted by the corresponding solid curves based on Eq. (2) with R^2 (the goodness of fit) all superior to 0.99. Initially, the responses with various δB_z's are zero by subtracting their offset values. At $t = 1$ s, a step magnetic-field $B_y = 0.32$ nT (green curve) is applied, and the response signals begin to oscillate and approach steady state within seconds. The steady state values are different, $\delta S = 0$ for $\delta B_z = 0$, $\delta S > 0$ for $\delta B_z = 50$ nT, and $\delta S < 0$ for $\delta B_z = -50$ nT. That means B_y is compensated in steady state at the compensation point $\delta B_z = 0$, whereas B_y still results in an output signal in steady state with other δB_z's.

458 K, the densities of K and Rb atoms are about 3.8×10^{12} and 3×10^{14} cm^{-3}, respectively. Utilizing the magnetic-field zeroing procedures [15], B_c is found to be 287.5 nT with the pump light power density 335 mW/cm^2. In addition, $R^e_{\rm tot}/\gamma_e$ is measured to be 31.84 nT by fitting the linewidth of the dispersion curve in Fig. 4 at 458 K.

In the self-compensation regime, the steady signal of the comagnetometer measures rotation only. We use the projection of earth rotation on the horizontal plane (maximum 5.59×10^{-5} rad/s) as an input signal to calibrate the signal. As shown in Fig. 5, the Y axis of the comagnetometer is initially aligned with the east direction and counterclockwise rotated 30° each time. After accomplishing each heading angle rotation, the steady signal is measured. These measured signals are fitted nicely with the sinusoidal curves. The coefficients of determination R^2 (the goodness of fit) are superior to 0.99. The maximal signals appear when the Y axis is directed along the north-south position where the projection of earth rotation reaches the maximum. Although the fitting curves feature phase shifts of 14° for pump power 335 mW/cm^2 and $-7°$ for 272 mW/cm^2, respectively, which probably results from residual cross talk from Ω_x. A sensitivity of 2.1×10^{-8} rad s^{-1} Hz$^{-1/2}$ has been achieved based on the K-Rb-^{21}Ne comagnetometer, which shows that the comagnetometer could be applied in the precision rotation measurement [18].

To verify the simultaneous measurement, we rotate the rotation platform to the direction with $\Omega_y = 0$ and input a step magnetic field along the Y axis with amplitude $B_y = 0.32$ nT to calibrate the system parameters λ_1, λ_2. At the compensation point, a typical signal of the comagnetometer is shown by the black curve in Fig. 6. The response of the comagnetometer can be divided into two parts: a fast decay oscillation signal and a steady signal. As a result of the self-compensation of the transverse magnetic field by the magnetization of ^{21}Ne, the steady signal equals zero no matter that there is a magnetic-field input along the Y axis at the compensation point. The fast decay oscillation signal can be fitted with Eq. (2), which gives $\lambda_{1i} = -5.02 \pm 0.09$, $\lambda_{1r} = -39.4 \pm 0.7$, $\lambda_{2i} = -0.92 \pm 0.02$, and $\lambda_{2r} = -1.46 \pm 0.04$.

After the calibration of λ_1, λ_2, we then simultaneously measure different B_y's and Ω_y's where the step magnetic fields are generated by the coils and the rotation along the Y axis is produced by the projection of earth rotation. The results are plotted in Fig. 7 in which Ω_y ranges from -4.01×10^{-5} to 5.37×10^{-5} rad/s, and B_y ranges from 0.048 to 0.128 nT. The points represented in black and red are measured as P_{1r} and $S_x^{\rm steady}$, respectively, and the colored planes are the fits to the data. According to Eq. (3), P_{1r} is linearly dependent on

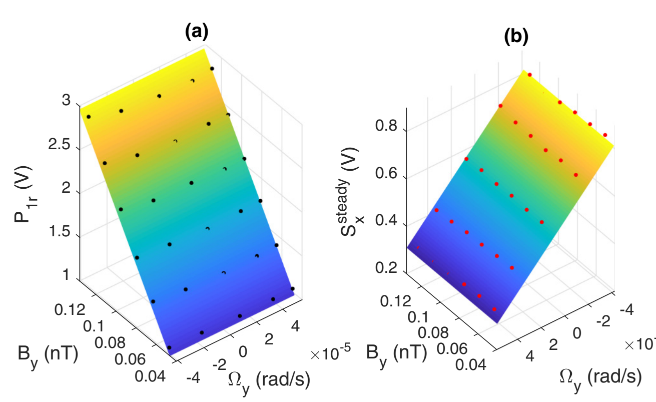

FIG. 7. The fitted P_{1r} and $S_x^{\rm steady}$ as functions of the angular velocity and magnetic field. The points represented in red and black are measurement points, and the colored planes are the fit to the data. The fitting functions of the subgraphs are $P_{1r} = 21.86B_y - 0.0124$ and $S_x^{\rm steady} = -5124\Omega_y + 0.6048$, respectively.

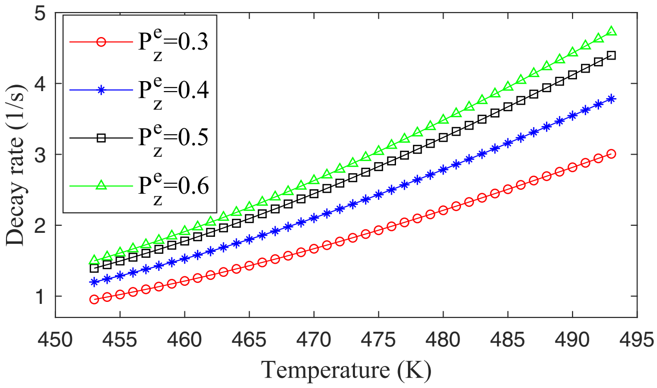

FIG. 8. Simulations of relationship between λ_{1r} and temperature as well as the polarization of Rb electrons P_z^e.

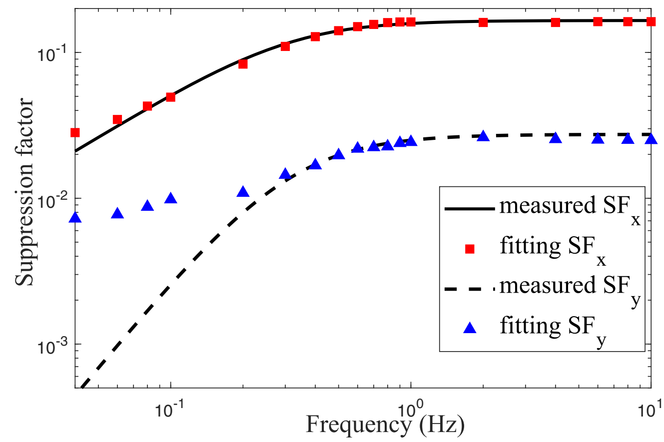

FIG. 9. Suppression of the comagnetometer response to oscillating fields along the X axis and the Y axis.

B_y and Ω_y, whereas the measured P_{1r} is linearly dependent on B_y but not significantly affected by Ω_y in Fig. 7(a) with the relationship of $P_{1r} = 21.86B_y - 0.0124$ because $K_\Omega\Omega_y$ are several orders of magnitude smaller than K_BB_y according to Eqs. (6) and (7). In Fig. 7(b), there is a linear relationship between $S_x^{\rm steady}$ and Ω_y, $S_x^{\rm steady} = -5124\Omega_y + 0.6048$ as expected in Eq. (4), whereas $S_x^{\rm steady}$ is independent of B_y due to the nuclear magnetization compensating the magnetic field in steady state. We also verify that the fitting parameters remain constant in different B_y and Ω_y inputs. The measurement accuracy of the magnetic field is 0.01 nT, and the measurement accuracy of rotation is 2×10^{-5} rad/s, which are primarily limited by the technique noises in the system, such as power fluctuations of pump light, heating temperature stability.

Finally, we present the main limitations of this simultaneous measurement method. It is noted that the simultaneous measurement rate is limited by the decay rate of the transient process, which approximates to 1.46 1/s in this experiment. According to Eq. (2), there are two oscillation parts in the transient process $\lambda_1 = \lambda_{1r} + i\lambda_{1i}$ and $\lambda_2 = \lambda_{2r} + i\lambda_{2i}$, corresponding to precessions of Rb electrons and ^{21}Ne nuclei, respectively, with different decay rates and frequencies. The decay rate of the transient is determined by the slower decay rate λ_{1r},

$$\lambda_{1r} = \frac{-R_{\rm tot}^e}{2Q} + \frac{\sqrt{\sqrt{a^2+b^2}+a}}{2\sqrt{2}}, \tag{8}$$

$$a = \left(\frac{R_{\rm tot}^e}{Q}\right)^2 - \left(\gamma_e\frac{B_z^e}{Q} + \gamma_nB_z^n\right)^2, \tag{9}$$

$$b = 2\frac{R_{\rm tot}^e}{Q}\left(\gamma_e\frac{-B_z^e}{Q} + \gamma_nB_z^n\right) - \frac{4\gamma_eB_z^e\gamma_nB_z^n}{Q}. \tag{10}$$

The slower decay rate λ_{1r} is related to B_z^e, B_z^n, and $R_{\rm tot}^e$, which are further associated with temperature and Rb electron spin-polarization P_z^e. This theoretical model has been experimentally verified in our previous work [19]. As shown in Fig. 8, the relationships between λ_{1r} and temperature as well as P_z^e are simulated based on Eq. (8). λ_{1r} increases with increasing of temperature and P_z^e, thus, can be improved by optimizing these conditions. Furthermore, if we replace the ^{21}Ne atoms with ^{3}He atoms, λ_{1r} can increase by about one order of magnitude [11].

Another main limitation is that the simultaneous measurement relies on the self-compensating transverse magnetic field on steady state, whereas this compensation effect depends on the oscillation frequency of the magnetic field. The suppressions of the responses to the transverse magnetic fields with oscillation frequencies ω, B_x, and B_y, are defined by SF_x and SF_y, respectively,

$$SF_x = \frac{\omega}{\sqrt{\left(\gamma_nB_z^n\right)^2 + \left(\omega\gamma_e^2B_z^e/R_{\rm tot}^e\right)^2}}, \tag{11}$$

$$SF_y = \frac{\omega^2}{\left(\gamma_nB_z^n\right)^2 + \left(\omega\gamma_e^2B_z^e/R_{\rm tot}^e\right)^2}. \tag{12}$$

Figure 9 shows the measured results of suppression factors and the corresponding fitting curves based on Eqs. (11) and (12). The suppression factors SF_x and SF_y decrease with frequency, indicating a better suppression effect with lower frequency. The measured results of SF_y and the fitting curve are not coincident at lower frequency. This discrepancy is resulted from the fact that the responses to lower-frequency magnetic fields are strongly suppressed. Thus, the weak responses are severely affected by signal fluctuations and noises. In this experiment, the suppression effect is more significant underneath 1 Hz. The frequency limitation of this suppression effect results from the limitation of the precession rate of ^{21}Ne nuclear spins in the strongly coupled Rb-^{21}Ne spin ensembles, thus, the suppression ability could be enhanced by increasing the polarization of ^{21}Ne atoms P_z^n to achieve large B_z^n.

V. CONCLUSION

In conclusion, we have demonstrated a method of simultaneous measurement of the magnetic field and inertial rotation based on a K-Rb-^{21}Ne comagnetometer with the nuclear spin magnetization of the ^{21}Ne self-compensating magnetic field. The intuitive models of the hybrid hyperpolarization process and the principle of the self-compensation are present. The measurements of the projection of earth rotation on the horizontal plane from -5.59×10^{-5} to 5.59×10^{-5} rad/s from the steady signal and the measurements of the magnetic field ranging from 0.016 to 1.760 nT from the transient signal have been demonstrated, respectively. Furthermore, the simultaneous measurement of angular velocity ranging from -4.01×10^{-5} to 5.37×10^{-5} rad/s and the magnetic field ranging from 0.048 to 0.128 nT have also been demonstrated. Finally, we discuss the main limitations of this method and propose the potential improvement approaches.

This method features a real-time simultaneous measurement and can be potentially used in practical applications, such as precision measurements and navigations. In applications disturbed by transient and periodic magnetic fields, this method could be applied to measure the interference magnetic fields to reduce their influences during measurement of nonmagnetic signals, such as searching for anomalous forces and fields as well as navigation. Besides, the drift of δB_z will significantly degrade the operation of the SERF comagnetometer by reducing the self-compensation effect on suppressing the low-frequency interference magnetic field. The parameter λ_{1r}, acquired by fitting the transient signal to the step transverse magnetic field, is a function of δB_z and could be utilized to zero the drift of δB_z in real time to reduce the system error. This simultaneous measurement method accurately characters the transient process of comagnetometer with R^2 all superior to 0.99, thus, could be applied to study the dynamic of the coupled Rb-^{21}Ne spin ensembles. In our recent work [20] to search for new spin-spin-velocity-dependent force, there is fluctuation in the recorded signal when the rotation direction of $SmCo_5$ magnets is changed, which disturbs the measurement; although the $SmCo_5$ magnets are shielded, the magnetic-field leakage exists, possibly resulting from the fluctuation, thus the transient signal induced by this magnetic field can be potentially measured by our method to improve the measurement accuracy. Besides, in the experiments searching for an anomalous field based on comagnetometer, the anomalous field is assumed to couple to spins not proportional to their magnetic moment as a magnetic field but rather similar to the inertial rotation, thus this method might be potentially used to simultaneously measure the anomalous field and the magnetic field to reduce the system error induced by the magnetic field.

ACKNOWLEDGMENTS

This work was supported by the National Key R&D Program of China (Grant No. 2016YFB0501600), the Fundamental Research Funds for the Central Universities, and the National Natural Science Foundation of China (Grants No. 61773043, No. 61721091, and No. 61227902). The authors would like to thank Professor J. Fang for a beneficial discussion. The authors also thank Y. Hu for his helpful suggestion regarding this work.

[1] D. Budker and M. Romalis, Nat. Phys. **3**, 227 (2007).
[2] D. Budker, W. Gawlik, D. F. Kimball, S. M. Rochester, V. V. Yashchuk, and A. Weis, Rev. Mod. Phys. **74**, 1153 (2002).
[3] J. Kitching, S. Knappe, and E. A. Donley, IEEE Sens. J. **11**, 1749 (2011).
[4] H. B. Dang, A. C. Maloof, and M. V. Romalis, Appl. Phys. Lett. **97**, 151110 (2010).
[5] H. C. Huang, H. F. Dong, L. Chen, and Y. Gao, Appl. Phys. Lett. **109**, 062404 (2016).
[6] D. Sheng, A. R. Perry, S. P. Krzyzewski, S. Geller, J. Kitching, and S. Knappe, Appl. Phys. Lett. **110**, 031106 (2017).
[7] T. W. Kornack, R. K. Ghosh, and M. V. Romalis, Phys. Rev. Lett. **95**, 230801 (2005).
[8] R. J. Li, W. F. Fan, L. W. Jiang, L. H. Duan, W. Quan, and J. C. Fang, Phys. Rev. A **94**, 032109 (2016).
[9] M. Smiciklas, J. M. Brown, L. W. Cheuk, S. J. Smullin, and M. V. Romalis, Phys. Rev. Lett. **107**, 171604 (2011).
[10] W. Quan, Y. Li, and B. Q. Liu, Europhys. lett. **110**, 60002 (2015).
[11] T. W. Kornack and M. V. Romalis, Phys. Rev. Lett. **89**, 253002 (2002).
[12] E. Babcock, I. Nelson, S. Kadlecek, B. Driehuys, L. W. Anderson, F. W. Hersman, and T. G. Walker, Phys. Rev. Lett. **91**, 123003 (2003).
[13] S. R. Schaefer, G. D. Cates, T. R. Chien, D. Gonatas, W. Happer, and T. G. Walker, Phys. Rev. A **39**, 5613 (1989).
[14] R. K. Ghosh and M. V. Romalis, Phys. Rev. A **81**, 043415 (2010).
[15] T. W. Kornack, A Test of CPT and Lorentz Symmetry Using a K $-$ ^{3}He Co-magnetometer, Ph.D. thesis, Princeton University, 2005.
[16] W. Quan, K. Wei, and H. R. Li, Opt. Express **25**, 8470 (2017).
[17] H. Zhang, S. Zou, and X. Y. Chen, IEEE Trans. Magn. **52**, 4002906 (2016).
[18] Y. Chen, W. Quan, S. Zou, Y. Lu, L. H. Duan, Y. Li, H. Zhang, M. Ding, and J. C. Fang, Sci. Rep. **6**, 36547 (2016).
[19] J. C. Fang, Y. Chen, Y. Lu, W. Quan, and S. Zou, J. Phys. B: At., Mol. Opt. Phys. **49**, 135002 (2016).
[20] W. Ji, Y. Chen, C. B. Fu, M. Ding, J. C. Fang, Z. G. Xiao, K. Wei, and H. Y. Yan, Phys. Rev. Lett. **121**, 261803 (2018).